Probability Density Functions of the Enstrophy Flux in Two Dimensional Grid Turbulence

H. Kellay,[1] C. H. Bruneau,[2] and X. L. Wu[3]

[1]*Centre de Physique Moléculaire Optique et Hertzienne, Université Bordeaux I, 351 cours de la Libération, 33405 Talence Cedex, France*

[2]*Departement de Mathématiques appliquées, Université Bordeaux I, 351 cours de la Libération, 33405 Talence Cedex, France*

[3]*Department of Physics and Astronomy, University of Pittsburgh, Pittsburgh, Pennsylvania 15260*

(Received 9 April 1999)

Probability density functions of the enstrophy flux in two dimensional grid turbulence are found to be strongly non-Gaussian and can be mimicked by stretched exponential functions. Evidence of this behavior is found in experiments using turbulent soap films and numerical simulations. The enstrophy flux itself is found to be constant for a range of scales corresponding to the enstrophy cascade.

PACS numbers: 47.27.Gs, 67.40.Vs, 68.15.+e, 92.60.Ek

There are very few significant results pertaining to homogeneous isotropic turbulence that can be derived analytically from the Navier-Stokes equation. Perhaps the most famous one is the expression for the third moment $S_3(r)$ of the longitudinal velocity difference $\delta u(r)$ between two points separated by $\mathbf{r}$. An expression for this moment can be written down for three dimensional (3D) and two dimensional (2D) systems. One may think of S_3 as a flux of kinetic energy per unit mass. Its sign in three dimensional systems is negative at all r, but in 2D there is no such restriction [1]. This paper is concerned with an analogous expression that applies only in 2D [2,3], namely the first moment of the enstrophy flux $\bar{Q}(r)$ $[\equiv \langle Q(r)\rangle = \langle \delta u(r)\delta\omega^2(r)\rangle]$. The angular brackets indicate an ensemble average or time average, and $\delta f(r) = f(x + r, t) - f(x, t)$, where f can refer to the component of velocity $u(\mathbf{r}, t)$ along the line $\mathbf{r}$ or to the vorticity ω, which is a scalar in 2D. The square of the vorticity in 2D is called the enstrophy. For the properties of turbulence in 2D we refer the reader to Refs. [4–6].

Experimentally, one obtains $S_3(r) = \langle \delta u(r)^3\rangle$ and $\bar{Q}(r)$ from a measurement of the probability density function of these fluxes. In this contribution, we present and discuss our measurements of the probability density function for the 2D enstrophy flux, which seems not to have been measured before. Though we did not have good enough statistics to measure $\bar{Q}(r)$ itself, we have observed interesting features of the probability density $P(Q(r))$, of the enstrophy flux $Q(r)$. In 2D turbulence, vorticity gradients are amplified by random advection [4]. If the Reynolds number Re of the flow is significantly large, a steady state can be established over a range of scales defined by $\ell_d < r < \ell_0$, where $\ell_d = \sqrt{\nu/\beta^{1/3}}$ is the Kolmogorov dissipation scale for enstrophy and ℓ_0 is the injection scale if the turbulence is forced or the outer scale if the turbulence is freely decaying. Within this so-called enstrophy subrange $\ell_d < r < \ell_0$, it can be shown that $\bar{Q}(r) = -2\beta r$ with $\beta = \nu\langle(\nabla\omega)^2\rangle$ being the mean enstrophy dissipation rate and ν the kinematic viscosity [2].

In a fast moving soap film which is rendered turbulent by the insertion of a grid, we measured the local velocity $\mathbf{u}(\mathbf{r}, \mathbf{t})$ and vorticity $\omega(\mathbf{r}, t)$ using a novel fiber velocimeter [7–9]. Our principal finding is that the probability density functions $P(Q(r))$ are strongly non-Gaussian, even at scales much larger than the production scale (i.e., the tooth spacing of the comb). This behavior is contrary to that exhibited by the probability density function for velocity increments measured in both 3D systems [10] and in 2D systems [1,11]. Our measurements also show a significant range of spatial scales r, where $P(Q(r))$ is independent of r once $Q(r)$ is rescaled by r: the probability density function $P(Q(r)/r)$ has the same functional form for all r in the interval $2 < r < 12$ mm. This leads us to state that the moments of order n of Q scale as r^n, which is consistent with the variation of the absolute moment of the enstrophy flux with the increment r.

The experiments were carried out in a vertical soap film formed between two parallel thin wires, as described in Refs. [7,8,12]. The use of soap films to produce two dimensional flows has been pioneered by Couder *et al.* [13] and Gharib and Derango [14]. The channel has a length of 2 m and a width of 5.5 cm. Soapy water was pumped from a reservoir to the top of the channel with a variable speed micropump which has a range of flow rates from less than 0.1 to 1 ml/s. The film falls under the action of gravity at speeds controlled by the injection flux. We used a commercial detergent at a concentration of about 2% in water for the soap solution. The channel frame was made of nylon wires of diameter 0.8 mm, which were draped over hooks for support with a weight suspended at the bottom end to tighten the frame. We use a comb with seven cylindrical teeth of 3.5 mm diameter and 7 mm spacing between the teeth. The films obtained with this channel can last for several hours without breaking. For the measurements presented here, the mean film thickness was about 6 μm and the mean speed was about 2 m/s with a turbulent intensity (at 6 cm below the grid) of about 15% as measured by laser Doppler velocimetry. With such a channel, several interesting results were reported on the velocity spectra,

 0031-9007/00/84(8)/1696(4)$15.00 © 2000 The American Physical Society

velocity differences [7], vorticity spectra [8], and on the moments of velocity increments [1]. Although the results seem to be consistent with expectations for 2D decaying turbulence [15], some deviations were observed [1,8]. Our own numerical simulations of a similar situation as the experiments captured the main features of these experiments on soap films [16].

For the measurements presented here both the vorticity and the velocity need to be measured simultaneously. This is achieved by using a novel velocimeter developed recently for the study of two dimensional flows with soap films [7,8]. For the measurement of the vorticity, two of these velocimeters are used as they provide an almost instantaneous determination of both the longitudinal and transverse components of the velocity at the two different locations [8]. Each velocimeter consists of a short optical fiber, one end of which penetrates about 0.5 mm through the film and which is deflected by the film flow. The output of a small laser is connected to the far end of the fiber, producing a somewhat diffuse spot at the deflecting end. The $x(t)$ and $y(t)$ deflections of this spot are measured by a position-sensitive detector and recorded in a computer. Independent measurements establish that the vertical and horizontal deflections are proportional to the y and x components of the velocity [9]. This linearity of the fiber response requires that one is below the resonance frequency f_0 of the fiber deflection. With the fibers used here, diameter $= 60$ μm and length $= 0.7$ cm, f_0 was 1.5 kHz.

To measure the vorticity fluctuations we use two velocity probes at the same vertical position and separated horizontally by a small distance Dx (typically 1 mm) to measure the velocity in two different points in the flow. The vorticity is constructed from the measured velocity in two different locations: both components of the velocity are needed at different positions simultaneously. Recall that the vorticity for a two dimensional flow is given by $\omega = dv_y/dx - dv_x/dy$, where v_x and v_y are, respectively, the transverse and longitudinal components of the velocity. The first derivative term, for a small Dx, is taken as the difference between the longitudinal velocities at the two horizontal points. The second derivative term is constructed using the frozen turbulence assumption: the transverse component is measured at time t and time $t + Dt$ such that $\bar{V}Dt = Dy = Dx$ and the spatial derivative dv_x/dy is taken as $[v_x(t + Dt) - v_x(t)]/\bar{V}dt$ [8].

We also carried out simulations of the channel flow to test the validity of our results and their two dimensional nature. The numerical simulations use a two dimensional channel in which an array of five equally sized and equally spaced cylinders is introduced to perturb the flow in a similar fashion as the experiments. The Navier-Stokes equations are numerically solved for the channel geometry. The highest resolution of our simulations was $360 \times (3 \times 360)$. The channel width is normalized to 1, the velocity is also fixed to 1, while the viscosity is varied to achieve different Reynolds numbers. The channel length was 3 in units of channel width. The time step is 10^{-4} in these units and the runs had typical durations of 10^6 time steps. The array of cylinders was placed at a length of one channel width from the entrance. The flow before the cylinders is laminar and displays a Poiseuille profile. The diameter of the cylinders used is 0.1 and the spacing between the cylinders is 0.2. These dimensions and geometry resemble the experimental conditions. These simulations take advantage of recent studies on incorporating obstacles and boundary conditions in incompressible two dimensional flows. Further details on the numerical techniques used can be found in the following references [17]. In Ref. [16] a study of the statistics of the velocity and the vorticity of this channel flow is presented. Good agreement is found with the experimental results using turbulent soap films.

In both the experiments and the simulations, the spatial increments for evaluating the vorticity were deliberately varied to test the sensitivity to the values used. No noticeable changes to the results were seen by doubling the resolution of the numerical simulations, and by changing the experimental Dx and Dy.

The increments of velocity and vorticity across a scale r are evaluated, in both experiments and numerical simulations, from a time series of the velocity or the vorticity; the difference is calculated by taking a variable time increment τ instead of a distance r. Here, by using the frozen turbulence assumption, one can identify this time increment with a distance r by multiplying the time increment by the mean velocity of the flow. In experiments this is a convenient way to calculate these increments especially for the vorticity, as it is very difficult to use several vorticity probes. The experiments and simulations can be compared directly. For an experimental test of the frozen turbulence assumption please refer to [18].

To calculate the enstrophy flux $Q(r)$, the vorticity and the longitudinal velocity were measured at the same position and a time trace is obtained from which we extract this quantity. For the experiments, the longitudinal velocity used is an average over the four velocities measured, but using only one of these velocities gives similar results. Typical experimental results are shown in Fig. 1 for the probability density function (pdf) $P(Q(r))$ at different spatial separations r. The pdfs recorded for different separations r have widths which increase as the separation increases. These pdfs are strongly non-Gaussian and present long tails for large values of the flux. Curiously, the enstrophy cascade is believed to be nonintermittent [19]. Another interesting point is that the pdfs are roughly symmetric. The relation stated above for the enstrophy flux predicts asymmetry of the pdfs. However, our measurements indicate that this asymmetry must be small and is difficult to measure. Further, we find that the $P(Q(r))$ can be mimicked by a stretched exponential function $\exp\{-[\mathrm{abs}(Q(r))/Q_0]^{\alpha}\}$. This is shown in Figs. 2a and 2b for the experimental results and the numerical simulations, respectively. This fit works well for the entire

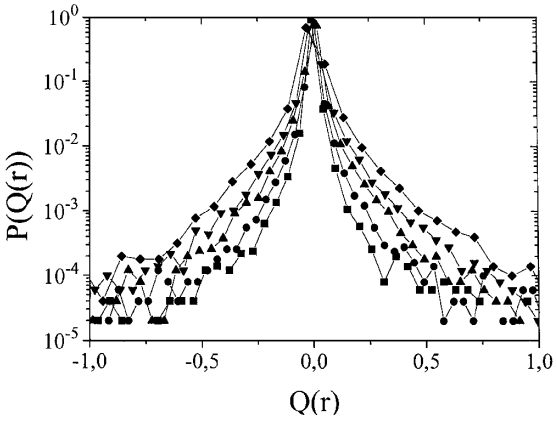

FIG. 1. Experimental probability density functions for $\delta u(r)\delta\omega^2(r)$ for different values of r. $r = 0.2$ cm (squares), 0.4 cm (circles), 0.6 cm (up triangles), 0.8 cm (down triangles), and 1 cm (diamonds). The measurements are carried out at a distance of 6 cm from the grid.

range of $Q(r)$ covered in the experiment. In addition, the value of α is 0.4 for both the experiment and the numerical simulations with little variation as r is varied.

Results from 3D turbulence experiments [20,21] have also found the pdfs of velocity increments to be non-Gaussian. These pdfs can be fit to stretched exponentials with exponents varying from about 0.5 at small scales (including the dissipative range) to 2 at scales comparable or greater than the integral scale of the turbulence. While the functional shape of the pdfs is similar to the ones we find for the enstrophy flux, we have not observed systematic changes of the exponent with scale as in 3D experiments. Perhaps, one needs to look at the pdfs of $\delta u(r)^3$ in 3D to make a comparison with our results since the analog of the enstrophy flux is the energy injection rate in 3D.

To gain more insight into how $P(Q(r))$ varies as a function of the separation r we plot the pdfs in Figs. 3a and 3b, for the experimental and the numerical results, respectively, with a rescaling of the horizontal axis as $\delta u(r)\delta\omega^2(r)/r = Q(r)/r$. The collapse of the pdfs for different separations on one single curve clearly indicates that $P(Q(r)/r)$ is independent of r to within the precision of the measurements. This collapse works only for separations between about a twentieth and a third of the channel width. This collapse does not carry over to larger separations nor to smaller ones. This is our principal finding which points to the possibility that the moments of order n of $Q(r)$ scale as r^n in the interval where the pdfs can be collapsed. Here it suffices to note that since $P(Q(r)/r)$ is

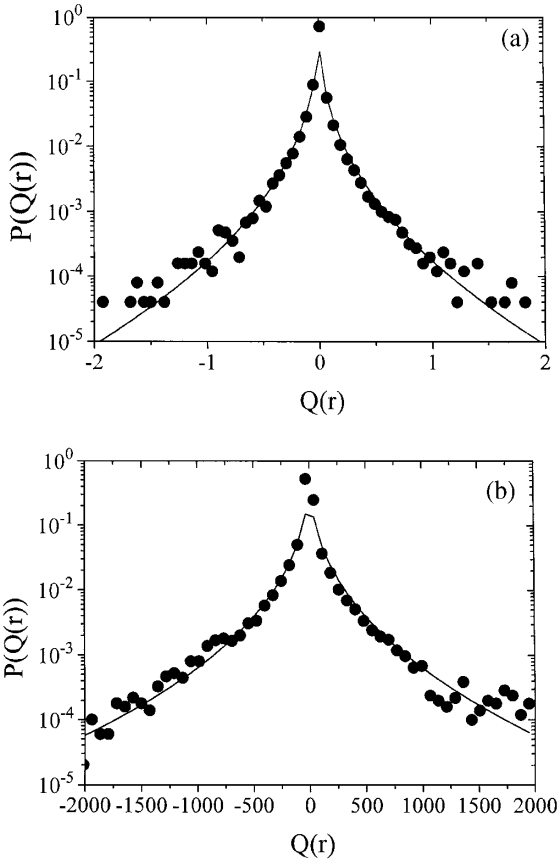

FIG. 2. (a) Experimental pdfs for $\delta u(r)\delta\omega^2(r)$ and a fit using a stretched exponential function with an exponent of 0.41 ($r =$ 1 cm). (b) pdfs for $\delta u(r)\delta\omega^2(r)$ from the numerical simulations for a Reynolds number (Re) of 5×10^5 ($r = 0.06L$) along with a stretched exponential fit with an exponent of 0.4.

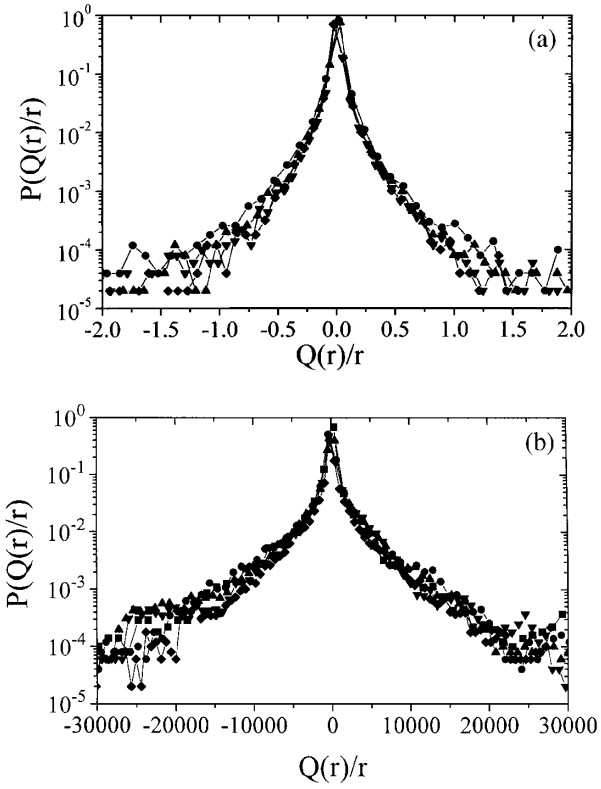

FIG. 3. (a) Experimental rescaled pdfs for $\delta u(r)\delta\omega^2(r)$: the horizontal axis has been divided by r. $r = 0.4$ cm (circles), 0.6 cm (up triangles), 0.8 cm (down triangles), and 1 cm (diamonds). (b) rescaled pdfs for $\delta u(r)\delta\omega^2(r)$ from the numerical simulations (Re $= 5 \times 10^5$: the horizontal axis has been divided by r. $r = 0.05L$ (squares), $0.095L$ (circles), $0.14L$ (up triangles), $0.185L$ (down triangles), $0.23L$ (diamonds). L is the channel width.

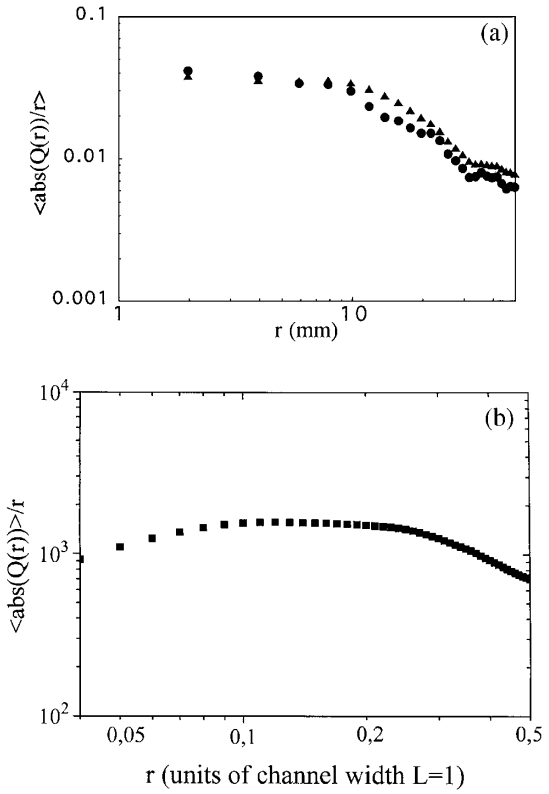

FIG. 4. (a) Experimental results of the variation of $\langle \|\delta u(r)\delta\omega^2(r)\|\rangle/r$ versus r. (b) Numerical results (Re $= 5 \times 10^5$) of the variation of $\langle \|\delta u(r)\delta\omega^2(r)\|\rangle/r$ versus r.

independent of r, the moments of $Q(r)/r$ are also independent of r which leads to the above statement about the variation of the moments of $Q(r)$ versus r. This is born out by the dependence of the absolute moment of $Q(r)$ on r as we show below. The absolute moment of $Q(r)$ compensated by dividing by r is displayed in Figs. 4a and 4b for the experiments and the simulations, respectively. As can be seen from these figures, the compensated absolute moment of Q shows a flat part for a significant range of scales: typically from 0.2 to 1.2 cm (which corresponds to the enstrophy cascade range of scales as determined previously [1,8]) for the experimental data and from 0.08 to $0.25L$ for the numerical simulations (which also corresponds to the enstrophy range [16], L is the channel width). We display the absolute moment of $Q(r)$ since our statistics do not allow us to measure odd moments. Nonetheless, this finding is in agreement with recent results [22] and confirms at least partially the relation stated above for $Q(r)$. This may be evidence that for the range of scales where the collapse of the pdfs is successful the enstrophy transfer rate β is constant as would be expected for the enstrophy cascade range of 2D turbulence. One of our most puzzling observations concerns the long tails of the pdfs of the enstrophy flux. The reasonable fit using a stretched exponential fit gives a stretching exponent of 0.4 for both the numerical simulations and the experimental data. A pressing question is the origin of such a functional shape of the pdfs. Despite the presence of such long tails for the pdfs of the enstrophy flux, a good collapse can be obtained for a range of scales showing that by a proper rescaling of the $Q(r)$ axis the pdfs become independent of r even for large departures from the mean value, i.e., at the tails of the pdfs.

In summary, measurements and numerical simulations show that the probability density functions of the enstrophy flux for different spatial scales in two dimensional turbulence are non-Gaussian and can be mimicked by stretched exponential functions. While we know of exact calculations in two dimensions which show that the first moment should scale as r, we know of no results which predict the functional shape of the pdfs. Our results for the absolute first moment of the enstrophy flux suggest that this moment is linear in the spatial increment used.

We are grateful to W. I. Goldburg and A. Belmonte for several discussions.

[1] A. Belmonte, W. I. Goldburg, H. Kellay, M. A. Rutgers, B. Martin, and X. L. Wu, Phys. Fluids **11**, 1196 (1999).
[2] E. Lindborg, J. Fluid Mech. **326**, 343–356 (1996).
[3] G. L. Eyink, Phys. Rev. Lett. **74**, 3800 (1995).
[4] G. K. Batchelor, Phys. Fluids Suppl. II **12**, 233 (1969).
[5] R. Kraichnan, Phys. Fluids **10**, 1417 (1967).
[6] M. Lesieur, *Turbulence in Fluids* (Kluwer Academic Publishing, Dordrecht, 1990), 2nd ed.
[7] H. Kellay, X-l. Wu, and W. I. Goldburg, Phys. Rev. Lett. **74**, 3975 (1995).
[8] H. Kellay, X. L. Wu, and W. I. Goldburg, Phys. Rev. Lett. **80**, 277 (1998).
[9] M. Rivera *et al.*, Rev. Sci. Instrum. **69**, 3215 (1998).
[10] U. Frisch, *Turbulence* (Cambridge University Press, Cambridge, England, 1995).
[11] J. Paret and P. Tabeling, Phys. Fluids **10**, 3126 (1998).
[12] M. Rutgers, X-l. Wu, R. Bagavatula, A. A. Peterson, and W. I. Goldburg, Phys. Fluids **8**, 2847 (1997).
[13] Y. Couder, J. Phys. Lett. **45**, L-353 (1984); Y. Couder, J. M. Chomaz, and M. Rabaud, Physica (Amsterdam) **37D**, 384 (1989).
[14] M. Gharib and P. Derango, Physica (Amsterdam) **37D**, 406 (1989).
[15] J. R. Chasnov, Phys. Fluids **9**, 171 (1997).
[16] C. H. Bruneau, O. Greffier, and H. Kellay, Phys. Rev. E **60**, R1162 (1999).
[17] C. H. Bruneau and P. Fabrie, Math. Model Numer. Anal. **30**, 815 (1996); Int. J. Numer. Methods Fluids **19**, 693 (1994); C. H. Bruneau, Comp. Fluid Dyn. Rev. **1**, 114 (1998); Ph. Angot, C. H. Bruneau, and P. Fabrie, Numer. Math. **11**, 1196 (1999).
[18] A. Belmonte *et al.* [Phys. Fluids (to be published)].
[19] A. Babiano, B. Dubrulle, and P. Frick, Phys. Rev. E. **52**, 3719 (1995).
[20] P. Kailasnath, K. R. Sreenivasan, and G. Stolovitzky, Phys. Rev. Lett. **68**, 2766 (1992).
[21] P. Tabeling *et al.*, Phys. Rev. E **53**, 1613 (1996).
[22] M. Rivera, P. Vorobieff, and R. E. Ecke, Phys. Rev. Lett. **81**, 1417 (1998).